

# High-Quality Image Restoration from Partial Random Samples in Spatial Domain

Jian Zhang<sup>a</sup>, Ruiqin Xiong<sup>b</sup>

<sup>a</sup>School of Computer Science and Technology  
Harbin Institute of Technology, Harbin, China  
Email: {zhangjian, rqxiong}@jdl.ac.cn

Siwei Ma<sup>b</sup> and Debin Zhao<sup>a</sup>

<sup>b</sup>Institute of Digital Media  
Peking University, Beijing, China  
Email: {swma, dbzhao}@jdl.ac.cn

**Abstract**—In this paper, a novel algorithm for high-quality image restoration is proposed. The contributions of this work are two-fold. First, a new form of minimization function for solving image inverse problems is formulated via combining local total variation model and nonlocal adaptive 3-D sparse representation model as regularizers under the regularization-based framework. Second, a new Split-Bregman based iterative algorithm is developed to solve the above optimization problem efficiently associated with proved theoretical convergence property. Experimental results on image restoration from partial random samples have shown that the proposed algorithm achieves significant performance improvements over the current state-of-the-art schemes and exhibits nice convergence property.

## I. INTRODUCTION

As a fundamental problem in the field of image processing, image restoration aims to reconstruct the original high quality image  $\mathbf{x}$  from its degraded observed version  $\mathbf{y}$ . It is a typical ill-posed linear inverse problem, which can be generally formulated as:

$$\mathbf{y} = \mathbf{H}\mathbf{x} + \mathbf{n} \quad (1)$$

where  $\mathbf{X}, \mathbf{Y}$  are lexicographically stacked representations of the original image and the degraded image, respectively,  $\mathbf{H}$  is a matrix representing a non-invertible linear degradation operator and  $\mathbf{n}$  is usually additive Gaussian white noise.

It has been widely recognized that image prior knowledge plays a critical role in the performance of image restoration algorithms. In order to cope with the ill-posed nature of image restoration, one type of scheme in literature employs image prior knowledge for regularizing the solution to the following minimization problem [1, 2]:

$$\min_{\mathbf{x}} \frac{1}{2} \|\mathbf{H}\mathbf{x} - \mathbf{y}\|_2^2 + \lambda \cdot \varphi(\mathbf{x}) \quad (2)$$

where  $\frac{1}{2} \|\mathbf{H}\mathbf{x} - \mathbf{y}\|_2^2$  is the so-called  $l^2$  data-fidelity term,  $\varphi(\mathbf{x})$  denotes an image prior named the regularization term and  $\lambda$  is the regularization parameter. In fact, the above regularization-based formulation (2) can be strictly derived from Bayesian Inference framework with prior knowledge as some image prior possibility model.

In this paper, we concentrate on one of the interesting problems in image restoration, where the original  $\mathbf{x}$  is masked

with a random mask, that is,  $\mathbf{H}$  is a diagonal matrix whose diagonal entries are randomly either 1 or 0, keeping or killing the corresponding pixels. What is required to do is the so-called image restoration from partial random samples in spatial domain (IRPRS).

To deal with the problem of IRPRS, local smoothness and nonlocal sparsity are both employed as image prior knowledge in our scheme. Specifically, we first incorporate local total variation model and nonlocal adaptive 3-D sparse representation model into the regularization-based framework simultaneously. This leads to a novel form of minimization problem, which can be considered as a combination of observation constraint, image local constraint and nonlocal constraint. And then, a new Split-Bregman based iterative algorithm with proved convergence is proposed to solve the above optimization problem efficiently. Our experimental results have shown significant performance improvements over the current state-of-the-art methods, demonstrating the potential of the proposed scheme.

The remainder of this paper is organized as follows. Section II gives the details of the proposed scheme, showing how local and nonlocal constraints are incorporated into the regularization-based framework to generate a new form of minimization function for image restoration and how the optimization problem is solved effectively with proved convergence. Experimental results are reported in Section III and Section IV ends the paper with a few remarks and pointers to future work.

## II. THE PROPOSED SCHEME UTILIZING BOTH LOCAL AND NONLOCAL CONSTRAINTS AS REGULARIZATIONS

In this section, we first introduce the local and nonlocal constraints, which will be incorporated into our proposed scheme as regularizations. After that, a new form of minimization function for image restoration under regularization-based framework is designed. Finally, a new effective algorithm for solving the above optimization problem with proved convergence is proposed.

### A. Local Total Variation Model

Total variation (TV) model is one of the most popular regularizers and has been widely used in recent year [7, 3, 2, 1]. Since the TV model favors the piecewise smoothness, this

---

This work is supported in part by National Science Foundation (No. 61073083 and 60803068), Beijing Natural Science Foundation (No. 4112026), Specialized Research Fund for the Doctoral Program of Higher Education (SRFDP) and National Basic Research Program of China (973 Program) under Grant 2009CB320904.

paper adopts the isotropic discrete total variation as one regularizer, which is expressed by

$$TV(\mathbf{x}) = \sum_i \sum_j \sqrt{(\Delta_{i,j}^h \mathbf{x})^2 + (\Delta_{i,j}^v \mathbf{x})^2}, \quad (3)$$

where  $\Delta_{i,j}^h \mathbf{x} \equiv \mathbf{x}_{i,j} - \mathbf{x}_{i,j-1}$  and  $\Delta_{i,j}^v \mathbf{x} \equiv \mathbf{x}_{i,j} - \mathbf{x}_{i-1,j}$  denote linear operators corresponding to horizontal and vertical first order differences at pixel  $\mathbf{x}_{i,j}$ , respectively.

### B. Nonlocal Adaptive 3-D Sparse Representation Model

Motivated by the success of sparse representation [11] and nonlocal means (NLM) [9, 10] in image restoration, we integrate them and introduce a nonlocal adaptive 3-D sparse representation model to better characterize nonlocal image model. Acting as a complement to local total variation model, nonlocal adaptive 3-D sparse representation model serves as the other regularizer that can be formulated in the following four steps.

Firstly, denote by  $\mathbf{x}[i]$  the  $i$ -th pixel and by  $\mathbf{X}_i$  the patch of size  $m$  centered on this pixel. Secondly, define for each patch  $\mathbf{X}_k$  the set of similar patches as

$$S_k = \{i = 1, \dots, n \text{ s.t. } \|\mathbf{x}_i - \mathbf{x}_k\|_2^2 \leq \xi\},$$

where  $\xi$  is some threshold. Thirdly, for every  $S_k$ , a group is formed by stacking the blocks belonging to  $S_k$  into a 3-D array, which is denoted by  $\mathbf{Z}_k$ . Finally, denote by  $\mathbf{T}^{3D}$  the operator of 3-D transform (e.g. 2-D Wavelet and 1-D DCT) and nonlocal adaptive 3-D sparse representation mode can be written as

$$\Psi_{3D}(\mathbf{x}) = \sum_k \|\mathbf{T}^{3D}(\mathbf{Z}_k)\|_1. \quad (4)$$

Different from BM3D [7], the nonlocal adaptive 3-D sparse representation model is expressed as an explicit formulation and can be interpreted from the joint sparse representation and nonlocal means point of view.

### C. Algorithm and Convergence

By incorporating local total variation model and nonlocal adaptive 3-D sparse representation model into the regularization-based framework, a new formulation for image restoration can be expressed as follows:

$$\arg \min_{\mathbf{x}} \frac{1}{2} \|\mathbf{H}\mathbf{x} - \mathbf{y}\|_2^2 + \tau \cdot TV(\mathbf{x}) + \lambda \cdot \Psi_{3D}(\mathbf{x}) \quad (5)$$

where  $\tau$  and  $\lambda$  are control parameters. Note that the formulation (5) can be interpreted as a combination of the data fidelity term and a compound regularization term, where the first actually represents the observation constraint and the second represents the image prior local and nonlocal constraints. Therefore, it is our belief that better results will be achieved by imposing the above three constraints into the ill-posed image inverse problem.

The next key is how to design algorithm to guarantee that the solution is a minimizer of (5) and stable. Recently, a so-called Split-Bregman iteration first introduced by [15] showing its efficiency for solving a class of  $l^1$  related

minimization problems. The connections of split Bregman iteration between some existing algorithms in optimization are pointed out by [12]. Founding on the Split-Bregman technique, in this paper, a modified iterative algorithm for solving (3) is then developed and its property of convergence property is presented as well.

Given a proper closed convex function  $g$  and any scalar  $t > 0$ , the proximal map associated to  $g$  is defined by

$$prox_t(g)(\mathbf{x}) := \underset{\mathbf{u}}{\operatorname{argmin}} \left\{ g(\mathbf{u}) + t \cdot \|\mathbf{u} - \mathbf{x}\|_2^2 \right\}. \quad (6)$$

By utilizing variable splitting technique [1, 14], the problem will change into a constrained optimization:

$$\underset{\mathbf{x}, \mathbf{z}, \mathbf{w}}{\operatorname{argmin}} \frac{1}{2} \|\mathbf{H}\mathbf{x} - \mathbf{y}\|_2^2 + \tau \cdot TV(\mathbf{z}) + \lambda \cdot \Psi_{3D}(\mathbf{w}) \quad (7)$$

s.t.  $\mathbf{x} = \mathbf{z}$  and  $\mathbf{x} = \mathbf{w}$ .

Obviously, equation (5) is equivalent to (7). The rationale behind variable splitting is that each step of this alternating minimization may be much easier than the original unconstrained problem (5), as will be seen below.

Applying Bregman algorithm [13, 14] to (7) leads to the following iterative steps:

$$(\hat{\mathbf{x}}^{(k+1)}, \hat{\mathbf{z}}^{(k+1)}, \hat{\mathbf{w}}^{(k+1)}) = \underset{\mathbf{x}, \mathbf{z}, \mathbf{w}}{\operatorname{argmin}} \frac{1}{2} \|\mathbf{H}\mathbf{x} - \mathbf{y}\|_2^2 + \tau \cdot TV(\mathbf{z}) + \lambda \cdot \Psi_{3D}(\mathbf{w}) + \mu_1 \cdot \|\mathbf{x} - \mathbf{z} - \mathbf{b}^{(k)}\|_2^2 + \mu_2 \cdot \|\mathbf{x} - \mathbf{w} - \mathbf{c}^{(k)}\|_2^2 \quad (8)$$

$$\mathbf{b}^{(k+1)} = \mathbf{b}^{(k)} - (\hat{\mathbf{x}}^{(k+1)} - \hat{\mathbf{z}}^{(k+1)}) \quad (9)$$

$$\mathbf{c}^{(k+1)} = \mathbf{c}^{(k)} - (\hat{\mathbf{x}}^{(k+1)} - \hat{\mathbf{w}}^{(k+1)}) \quad (10)$$

As mentioned before, Equation (8) can be performed efficiently by the alternating minimization with respect to  $\mathbf{X}, \mathbf{Z}$  and  $\mathbf{w}$  separately, and the complete algorithm proposed for solving (5) can be outlined in Table I.

TABLE I. A COMPLETE DESCRIPTION OF THE PROPOSED ALGORITHM

#### Initialization:

Set  $k = 0$ ,  $\mathbf{b}^{(0)} = \mathbf{c}^{(0)} = \mathbf{0}$ ,  $\hat{\mathbf{w}}^{(0)} = \hat{\mathbf{z}}^{(0)} = \mathbf{0}$ ,  $\mu_1, \mu_2, \tau, \lambda$

#### Main Loop:

Iterate on  $k$  until  $k = \text{MaxIterNum}$

$$\hat{\mathbf{x}}^{(k+1)} = \underset{\mathbf{x}}{\operatorname{argmin}} \left\{ \|\mathbf{H}\mathbf{x} - \mathbf{y}\|_2^2 + \mu_1 \cdot \|\mathbf{x} - (\mathbf{b}^{(k)} + \hat{\mathbf{z}}^{(k)})\|_2^2 + \mu_2 \cdot \|\mathbf{x} - (\mathbf{c}^{(k)} + \hat{\mathbf{w}}^{(k)})\|_2^2 \right\} \quad (11)$$

$$\tilde{\mathbf{z}}^{(k)} = \hat{\mathbf{x}}^{(k+1)} - \mathbf{b}^{(k)}; \quad \gamma = 2\tau / \mu_1; \quad (12)$$

$$\hat{\mathbf{z}}^{(k+1)} = prox_\gamma(TV)(\tilde{\mathbf{z}}^{(k)}) \quad (13)$$

$$\tilde{\mathbf{w}}^{(k)} = \hat{\mathbf{x}}^{(k+1)} - \mathbf{c}^{(k)}; \quad \eta = 2\lambda / \mu_2; \quad (14)$$

$$\hat{\mathbf{w}}^{(k+1)} = prox_\eta(\Psi_{3D})(\tilde{\mathbf{w}}^{(k)}) \quad (15)$$

$$\mathbf{b}^{(k+1)} = \mathbf{b}^{(k)} - (\hat{\mathbf{x}}^{(k+1)} - \hat{\mathbf{z}}^{(k+1)}) \quad (16)$$

$$\mathbf{c}^{(k+1)} = \mathbf{c}^{(k)} - (\hat{\mathbf{x}}^{(k+1)} - \hat{\mathbf{w}}^{(k+1)}) \quad (17)$$

Notice that the proposed algorithm can be essentially considered as a modified form of Split-Bregman method. In Table I,  $\mu_1, \mu_2, \tau, \lambda$  are pre-specified scalar parameters respectively, and  $MaxIterNum$  is the maximum number of main loops. Since (11) is a minimization problem of strictly convex quadratic function, there is a closed form for  $\hat{\mathbf{x}}^{(k+1)}$ , which can be expressed as

$$\hat{\mathbf{x}}^{(k+1)} = (\mathbf{H}^T \mathbf{H} + \mu \mathbf{I})^{-1} \cdot \mathbf{r}^{(k)} \quad (18)$$

where  $\mathbf{r}^{(k)} = \mathbf{H}^T \mathbf{y} + \mu_1 (\mathbf{b}^{(k)} + \mathbf{z}^{(k)}) + \mu_2 (\mathbf{c}^{(k)} + \mathbf{w}^{(k)})$ ,  $\mathbf{I}$  is identity matrix and  $\mu = \mu_1 + \mu_2$ . Owing to the particular structure of Matrix  $\mathbf{H}$  that satisfies  $\mathbf{H}\mathbf{H}^T = \mathbf{I}$ , applying the Sherman-Morrison-Woodbury (SMW) matrix inversion formula to (18) yields

$$\hat{\mathbf{x}}^{(k+1)} = \frac{1}{\mu} \left( \mathbf{I} - \frac{1}{1+\mu} \mathbf{H}^T \mathbf{H} \right) \cdot \mathbf{r}^{(k)}. \quad (19)$$

Therefore,  $\hat{\mathbf{x}}^{(k+1)}$  in (19) can be computed very efficiently without computing the matrix inverse operation in (18).

If (13) and (15) corresponding to the proximal maps associated to  $TV$  and  $\Psi_{3D}$ , respectively, are solved exactly, the convergence property of the proposed algorithm can be guaranteed by the following proposition.

**Proposition 1.** The proposed algorithm described by Table I converges to a minimizer of (5).

Due to the limits of space, the proof of proposition 1 is not provided here. Actually, the proximal maps associated to most functions can only be solved in an approximation way. In this paper, the proximal map associated to  $TV$  is approximated by the well-known Chambolle's algorithm [8], and the proximal map associated to  $\Psi_{3D}$  is calculated by applying thresholding (also called shrinkage) in transform domain of all the 3-D arrays centered at every pixel. However, it is important to stress that the approximations of (13) and (15) are found experimentally not to compromise the convergence of the proposed algorithm, which will be manifested in the next section.

### III. EXPERIMENTAL RESULTS

To evaluate the performance of the proposed algorithm, we compare it with a number of recent methods: KR (kernel regression) [5], FOE (fields of experts) [6], MCA (morphological component analysis) [4] and SALSA [1]. Four standard test images include: *House* (color, 256×256), *Barbara* (gray, 256×256), *Lena* (color, 512×512) and *Boat* (gray, 512×512), as shown in Figure. 1. The results of every color image are obtained by its luminance component, keeping its chrominance components unchanged. The experimental results of SALSA, KR, MCA and FOE are all generated by the original authors' codes, with the corresponding parameters manually optimized.

Table II lists Peak Signal to Noise Ratio (PSNR) results among different methods on test images. The second column represents the ratio of available data, i.e. the percentage of

retaining original samples, with the value equal to 20%, 50% or 80%. The proposed method considerably outperforms the other methods in all the cases, with a PSNR improvement of about 2.5 dB on average over the second best algorithms. With 50% available data on Image Barbara, which is rich in textures, the average PSNR improvements achieved by the proposed method over the second best method (i.e. MCA [4]) is as high as 4.8 dB.



Figure 1. Standard test images. From left to right: *House* (color, 256×256), *Barbara* (gray, 256×256), *Lena* (color, 512×512) and *Boat* (gray, 512×512).

Because of the limits of space, we merely provide two crops from Image *House* and *Barbara* for visual comparison in Figure 2. More visual results can be found at the website: <http://idm.pku.edu.cn/staff/zhangjian/IRPRS/>. It is apparent that all the methods generate good results on the smooth regions. KR [5] is good at capturing contour structures, but fails in recovering textures and produces blurred effects. MCA [4] can restore better textures than FOE [6] and KR. However, it produces noticeable striped artifacts. The proposed algorithm exhibits the best visual quality with the highest PSNRs, not only providing accurate restoration on both edges and textures but also suppressing the noise-caused artifacts.

To visually illustrate the convergence of the proposed algorithm, Figure 3 plots the evolutions of PSNR versus iterative numbers for the four test images when the ratio of available data is 80%. Each curve increases monotonically with the growth of iterative number and ultimately becomes flat, which fully demonstrates the convergence of the proposed algorithm.

TABLE II. PSNR (dB) COMPARISON AMONG DIFFERENT ALGORITHMS (BOLD-TYPE INDICATES THE BEST FOR EACH COLUMN)

Image and Data Ratio	SALSA	KR	MCA	FOE	Proposed	
<i>House (color)</i>	20%	29.55	30.4	32.22	32.64	<b>35.17</b>
	50%	35.32	36.75	38.65	39.21	<b>41.24</b>
	80%	41.28	43.95	44.44	45.91	<b>47.40</b>
<i>Barb. (gray)</i>	20%	23.55	23.31	25.81	24.62	<b>28.06</b>
	50%	27.28	31.50	32.14	31.66	<b>37.02</b>
	80%	33.48	39.51	39.37	39.79	<b>44.41</b>
<i>Lena (color)</i>	20%	30.41	32.84	31.59	32.15	<b>33.83</b>
	50%	35.75	38.19	37.17	37.84	<b>39.47</b>
	80%	41.83	43.34	42.72	43.55	<b>45.03</b>
<i>Boat (gray)</i>	20%	25.96	27.29	27.50	27.90	<b>28.99</b>
	50%	31.27	32.68	33.17	33.14	<b>34.82</b>
	80%	37.09	38.03	39.21	38.50	<b>40.84</b>
Average	32.73	34.82	35.33	35.58	<b>38.02</b>	

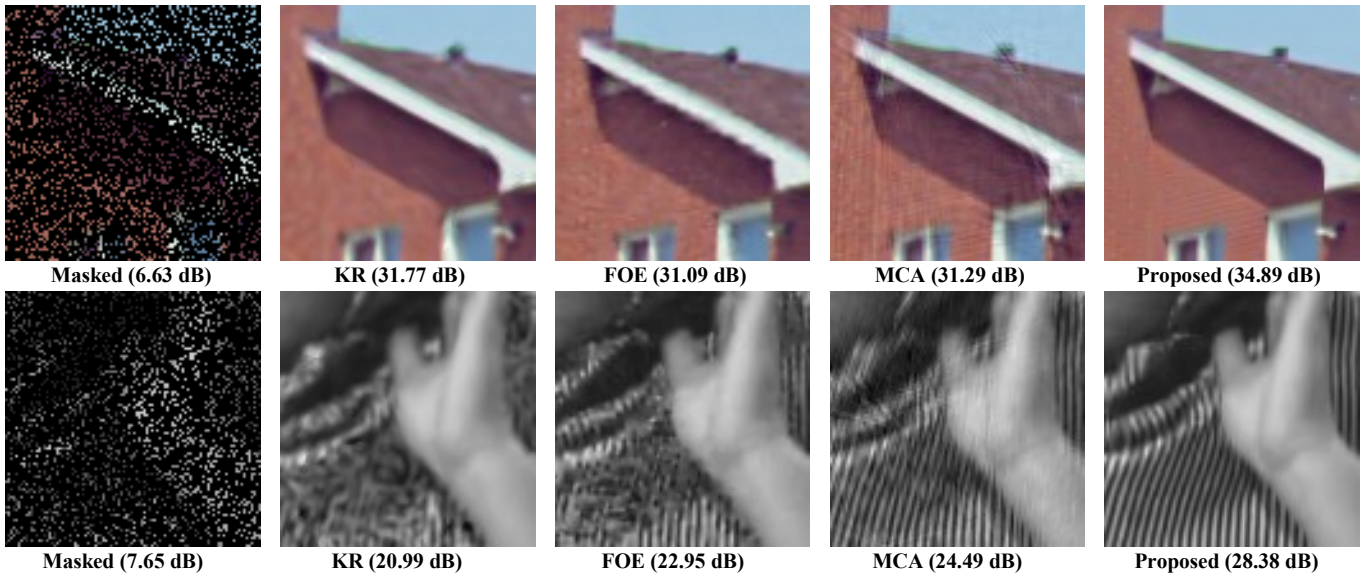


Figure 2. Visual comparison. Crops from two images (From top to bottom: *House* and *Barbara*). Left to right: masked image with only 20% random pixels available, KR [5], FOE [6], MCA [4] and the proposed algorithm. The reconstruction results of the proposed algorithm exhibit the highest image qualities.

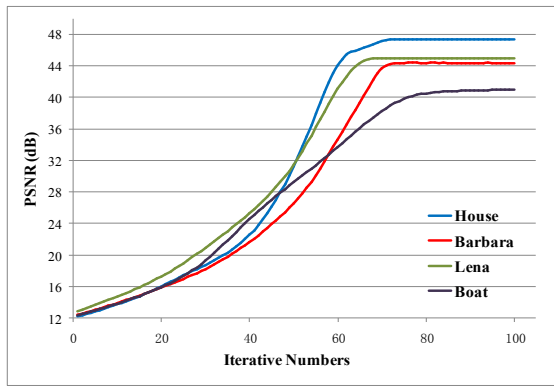


Figure 3. Evolutions of PSNR versus iterative numbers for the four test images when the ratio of available data is 80%. Each curve increases monotonically with the growth of iterative number and ultimately becomes flat, which fully demonstrates the convergence of the proposed algorithm.

#### IV. CONCLUSIONS

This paper presents a new scheme for image restoration, which consists of two steps. The first step formulates a novel optimization problem enforced simultaneously by observation constraint, local smoothness constraint and nonlocal sparsity constraint. The second step solves the above optimization problem efficiently using a new Split-Bregman based iterative algorithm, with proved convergence property. Encouraging outcomes are achieved by illustrating the proposed scheme on an interesting problem of IRPRS. Current and future work includes the extensions on a variety of applications, such as image deblurring, image denoising under impulse noise.

#### ACKNOWLEDGMENT

We would like to thank the authors of [1], [4], [5] and [6] for kindly providing their codes.

#### REFERENCES

[1] M. Afonso, J. Bioucas-Dias and M. Figueiredo, "Fast image recovery using variable splitting and constrained optimization," *IEEE Trans. on*

*Image Process.*, vol. 19, pp. 2345–2356, 2010.

[2] A. Beck and M. Teboulle, "Fast gradient-based algorithms for constrained total variation image denoising and deblurring problems," *IEEE Trans. on Image Process.*, vol. 18, pp. 2419–2434, 2009.

[3] J. Bioucas-Dias and M. Figueiredo, "A new TwIST: two-step iterative shrinkage/thresholding algorithms for image restoration," *IEEE Trans. on Image Process.*, vol. 16, pp. 2992–3004, 2007.

[4] M. Elad, J. L. Starck, P. Querre, and D.L. Donoho, "Simultaneous cartoon and texture image inpainting using morphological component analysis (MCA)," *Applied and Computational Harmonic Analysis*, vol. 19, pp. 340–358, 2005.

[5] H. Takeda, S. Farsiu, and P. Milanfar, "Kernel regression for image processing and reconstruction," *IEEE Trans. on Image Process.*, vol. 16, pp. 349–366, 2007.

[6] S. Roth and M. J. Black, "Fields of experts," *International Journal of Computer Vision*, vol. 82, pp. 205–229, 2009.

[7] K. Dabov, A. Foi, V. Katkovnik, and K. Egiazarian, "Image denoising by sparse 3D transform-domain collaborative filtering," *IEEE Trans. on Image Process.*, vol. 16, pp. 2080–2095, 2007.

[8] A. Chambolle, "An algorithm for total variation minimization and applications," *J. Math. Imaging Vis.*, vol. 20, pp. 89–97, 2004.

[9] A. Buades, B. Coll, and J. M. Morel, "A non-local algorithm for image denoising," *International Conference on Computer Vision and Pattern Recognition*, vol. 2, pp. 60–65, 2005.

[10] T. Brox, O. Kleinschmidt, and D. Cremers, "Efficient nonlocal means for denoising of textural patterns," *IEEE Transactions on Image Process.*, vol. 17, pp. 1083–1092, 2008.

[11] M. Elad and M. Aharon, "Image denoising via sparse and redundant representations over learned dictionaries," *IEEE Trans. on Image Process.*, vol. 15, pp. 3736–3745, 2006.

[12] E. Esser, "Applications of Lagrangian-based alternating direction methods and connections to split-Bregman," *Technical Report 09-31*, Computational and Applied Mathematics, University of California, Los Angeles, 2009.

[13] W. Yin, S. Osher, D. Goldfarb and J. Darbon, "Bregman iterative algorithms for  $\ell_1$ -minimization with applications to compressed sensing," *SIAM J. Imaging Sci.*, vol. 1, pp. 142–168, 2008.

[14] J. F. Cai, S. Osher, and Z. W. Shen, "Split Bregman methods and frame based image restoration," *Multiscale Model. Simul.*, vol. 8, pp. 5057–5071, 2009.

[15] T. Goldstein and S. Osher, "The Split Bregman Algorithm for  $L_1$  Regularized Problems," *SIAM J. Imaging Sci.*, vol. 2, pp. 323–343, 2009.